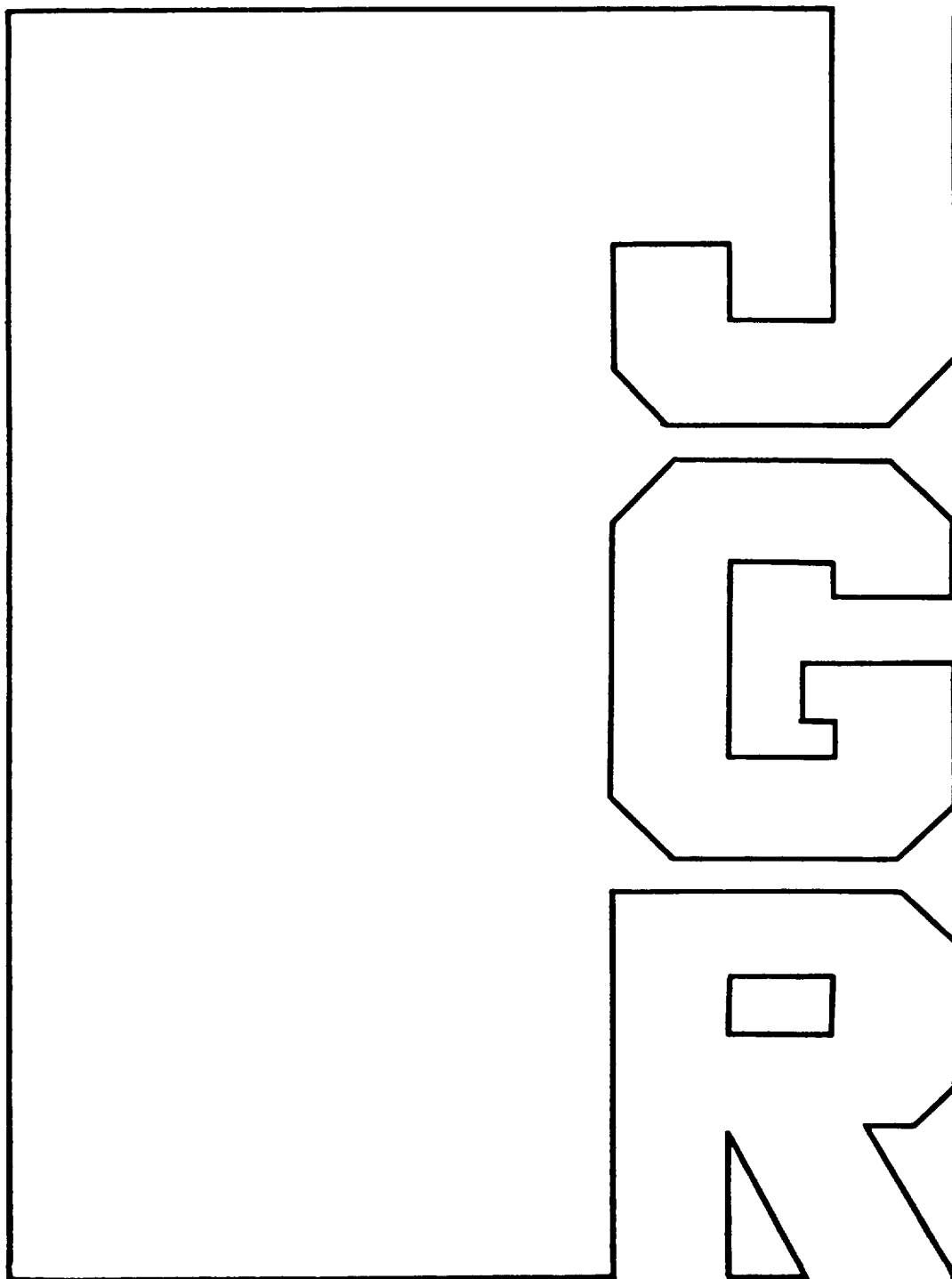


**Observation of local cloud and moisture feedbacks  
over high ocean and desert surface temperatures**

Moustafa T. Chahine





# Observation of local cloud and moisture feedbacks over high ocean and desert surface temperatures

Moustafa T. Chahine

Jet Propulsion Laboratory, California Institute of Technology, Pasadena, California

**Abstract.** New data on clouds and moisture, made possible by reanalysis of weather satellite observations, show that the atmosphere reacts to warm clusters of very high sea surface temperatures in the western Pacific Ocean with increased moisture, cloudiness, and convection, suggesting a negative feedback limiting the sea surface temperature rise. The reverse was observed over dry and hot deserts where both moisture and cloudiness decrease, suggesting a positive feedback perpetuating existing desert conditions. In addition, the observations show a common critical surface temperature for both oceans and land; the distribution of atmospheric moisture is observed to reach a maximum value when the daily surface temperatures approach  $304 \pm 1$  K. These observations reveal complex dynamic-radiative interactions where multiple processes act simultaneously at the surface as well as in the atmosphere to regulate the feedback processes.

## 1. Introduction

Prediction of greenhouse warming depends on knowledge of how clouds and atmospheric moisture interact with the surface and the general circulation of the atmosphere, a subject which has been widely debated [Charney, 1975; Lindzen, 1990; Ramanathan and Collins, 1991]. Not only is there no general theory to explain the interaction with precision, but we do not yet have the basic observational evidence required to validate such theories. This paper presents new observational data and discusses the implications for climate modeling with emphasis on two specific regions: warm ocean pools in the western Pacific and hot desert spots in Australia. The goal is to provide basic new information needed to improve our understanding of the processes which sustain the local surface temperatures of ocean and desert regions. Climate models with diverse approaches to parameterizing clouds and moist convection must be able to reproduce these observations as a test of their accuracy and ability to make reliable predictions.

Clouds and moisture show strong internal feedbacks and at the same time they can amplify and dampen the global and local energy balances. Clouds reflect solar energy and at the same time intercept long-wavelength radiation from the surface. The sign and amplitude of changes in the atmospheric and surface energy balances and the concurrent effect of atmospheric moisture on greenhouse warming are difficult to explain by radiation processes alone. Dynamical processes in the atmosphere exert controlling effects, as well. Accurate observations are needed, models must be refined and validated, and diverse mechanisms must be invoked to explain these phenomena [Chahine, 1992].

Since clouds and moisture vary rapidly as a function of space and time, it is necessary to observe them simultaneously in order to ascertain their links to each other and to the environment with which they interact. Although this has

been difficult in the past, the data set developed for this study used coincident observations from two instruments on the same satellite. The resulting global temperature, moisture, and cloud data simultaneously characterize the air mass and the underlying surface in each field of view. These characteristic parameters were analyzed daily during the months of January, April, July, and October 1979. The results discussed in this paper apply to the individual daily data as well as to their cumulative behavior. However, January was selected as the focus for this paper because it exhibited the largest clusters of warm spots. Furthermore, by confining the study to an individual month, the effects of changes in the global patterns of circulation are minimized.

In both the single-day data and the cumulative data we have observed that moisture increases at all atmospheric levels as a function of increased sea surface temperature (to  $\sim 304$  K). This increase in moisture above the boundary layer is most critical because of its strong positive feedback effect on greenhouse warming. Specifically, we have observed strong interactive processes between moisture and clouds over warm pools in the western Pacific. These interactive processes persist over long periods of time under various global and regional circulation patterns and appear to regulate the local environment through radiative-convective mechanisms. Over hot and dry desert areas, both moisture and cloudiness decrease as a function of increased surface temperature (above 304 K), providing a positive feedback mechanism which tends to maintain the desert conditions [Charney, 1975]. Intriguingly, the observations show a common critical surface temperature for both oceans and land; the distribution of atmospheric moisture is observed to reach a maximum value when the daily values of skin surface temperature approach  $304 \pm 1$  K.

## 2. Observations

The data derived for this study come from the high-resolution infrared sounder (HIRS) and the microwave sounding unit (MSU) flown on the NOAA low-Earth-orbiting operational weather satellites [Smith *et al.*, 1979] since

Copyright 1995 by the American Geophysical Union.

Paper number 95JD00094.  
0148-0227/95/95JD-00094\$05.00

December 1978. NOAA has derived global atmospheric temperature and moisture data since 1979. In the early years, NOAA analyzed the HIRS/MSU observations using a statistical approach [Smith and Woolf, 1976] which employed empirical relationships between satellite observations and atmospheric parameters gathered from radiosonde and rocket-sonde reports. However, the results of this approach do not meet the accuracy and consistency requirements of this study. To satisfy the study requirements, a completely analytical method [Chahine, 1972] was validated [Phillips *et al.*, 1988] and applied to reanalyze the HIRS/MSU observations [Susskind *et al.*, 1984], starting with the year 1979. The combined infrared and microwave observations permit both the "clear-sky" and the "cloudy-sky" properties of the atmosphere to be derived [Chahine, 1982] even though the atmosphere is never free from clouds and haze (see Appendix).

Specifically, the derived parameters consist of atmospheric profiles of temperature and precipitable water vapor (PWV), sea surface temperature (SST), land surface temperature (LST), the effective cloud infrared opacity ( $\alpha$ ), and the cloud top height and temperature. PWV is simply the mass of water vapor in a column of air bounded by two pressure levels. In any field of view,  $\alpha$  is defined as the fraction of radiance (between 8 and 15  $\mu\text{m}$ ) intercepted by the clouds, that is emitted by the surface and atmosphere below the clouds;  $\alpha$  can be roughly considered to be the product of the cloud emittance and cloud cover and in this spectral range it varies like the cloud cover [Chahine, 1982]. We define, also, the clear-sky radiance ( $F_{cl}$ ) as the radiance emitted by the surface and the atmosphere, that is transmitted through the clouds and through openings in the clouds. If we define the cloud radiance ( $C_{cd}$ ) as that emitted by the clouds and the atmosphere above them for full overcast conditions, we can then relate  $F_{cl}$  and  $C_{cd}$  to the observed radiance ( $F_{cd}$ ), i.e., the cloudy-sky radiance, as [Chahine, 1982]

$$F_{cd} = (1 - \alpha)F_{cl} + \alpha C_{cd} \quad (1)$$

It should be noted that the values of  $F_{cd}$  and  $F_{cl}$  may differ from those derived by the Earth Radiation Budget Experiment (ERBE). In ERBE, each field of view is assumed to be either cloudy or clear [Wielicki and Green, 1989], while in this paper the cloud opacity is individually determined in each field of view [Chahine, 1982]. For additional discussion, see Wu and Susskind [1990], Hartmann and Doelling [1991], and Kiehl and Briegleb [1992].

Linear kriging [Isaaks and Srivastava, 1989] was used to pinpoint regions of clusters of ocean warm pools and desert hot spots. Basically, linear kriging is a technique that gives more weight to, say, warm observations if they are close to each other than if they are far apart. As a result, linear kriging is very useful in image processing, as in Plate 1, particularly for enhancing the location of the (reddish) clusters of warm points as shown.

The accuracy of the data (see Appendix) for 1979 has been previously determined by careful comparison with in situ observations under diverse cloud and surface conditions [Chahine, 1974; Susskind and Reuter, 1985; Wu and Susskind, 1990; Barnett *et al.*, 1991]. An important limitation of this data set is that it does not contain the cloud properties in the visible part of the spectrum, because the visible channel on the HIRS instrument was not calibrated.

### 3. Warm Pacific Ocean Pools

The SST values derived from the space observations are the radiating temperature of the ocean "skin surface" and not the "bulk" SST values usually reported by ships. The diurnal variation of ocean skin surface temperature may differ from bulk temperature by about 1°C or more [Schluesel *et al.*, 1987]. The derived daily SSTs showed several clusters of warm water pools in the tropical Pacific between 20°N/20°S and 150°E/180°. A representative cluster to the northeast of Australia is shown in Plate 1 (top) for daytime observations on January 4, 1979. These warm pools were observed every day in January and October 1979 (Figures 1 and 2). They stretched across hundreds of kilometers and meandered slowly in the western Pacific, fluctuating slightly in size and intensity. A strong correlation was noted between changes in PWV and  $\alpha$  with the high SSTs. This correlation became weaker on certain days but never reversed its sign. Thus in this region of deep convection in the tropical western Pacific the warm pools and the air mass above cannot be considered in isolation from each other. The variations of the PWV as a function of daytime SST across the warm pools and the sea surrounding it are shown in Figures 1 and 2. Since the accuracy of the derived SST is estimated to be  $\pm 0.5^\circ\text{C}$ , a moving average of the corresponding values of PWV was calculated across an interval of  $0.5^\circ\text{C}$  in steps of  $0.05^\circ\text{C}$ . The standard deviation of the daily values of the total PWV in the intervals of high surface temperature was nearly constant at  $0.8 \pm 0.1 \text{ g/cm}^2$ . This running average reduced the noise (or scatter) of the individual daily observations of PWV by about 20%. The resulting "smoother" distributions correspond to variations of PWV in four layers bounded by 100, 300, 500, 700 mbar and the surface. The total PWV is given in Figures 1e and 2e. These results clearly show a very strong coupling between increases in moisture at all atmospheric levels and the increase in SST across the warm pools. Of distinct interest, the PWV at the higher altitudes increased faster than in any other atmospheric layer. For example, in Figure 1a, as the SST across the warm pools increased from 300 to 304 K, the PWV between 700 mbar and the surface increased by 20%, while the corresponding increase between 100 and 300 mbar was 100%. At SST values above 304 K the total PWV and  $\alpha$  decreased (Figures 1e and 2e). This trend was persistent and was observed frequently during each of the 4 months of this study with some variations in the slope of the decrease. However, between 700 mbar and the surface the PWV continued to increase at the rate of 1 to 2% per 1 K rise above 304 K, in January (Figure 1d) and April; this trend was neutral in July, then decreased in October (Figure 2d). Obviously, the selection of the 700-mbar level here is arbitrary and dictated by the sounding frequencies available on the HIRS instruments (higher vertical resolution in PWV is needed to determine if a rise in PWV occurred at lower levels also in October). Finally, it should be noted that in spite of the relatively small number of observations above 304 K the absolute count is large, corresponding to 992 data points in January (Figure 2f) and 1447 points in October (Figure 2f).

Figures 1e and 2e show the distribution of the corresponding effective cloud infrared opacity. The use of a moving average reduced the scatter of individual daily observation of  $\alpha$  by  $\pm 50\%$ . Below 300 K there is a negative correlation between cloud opacity and SST which was also noted by

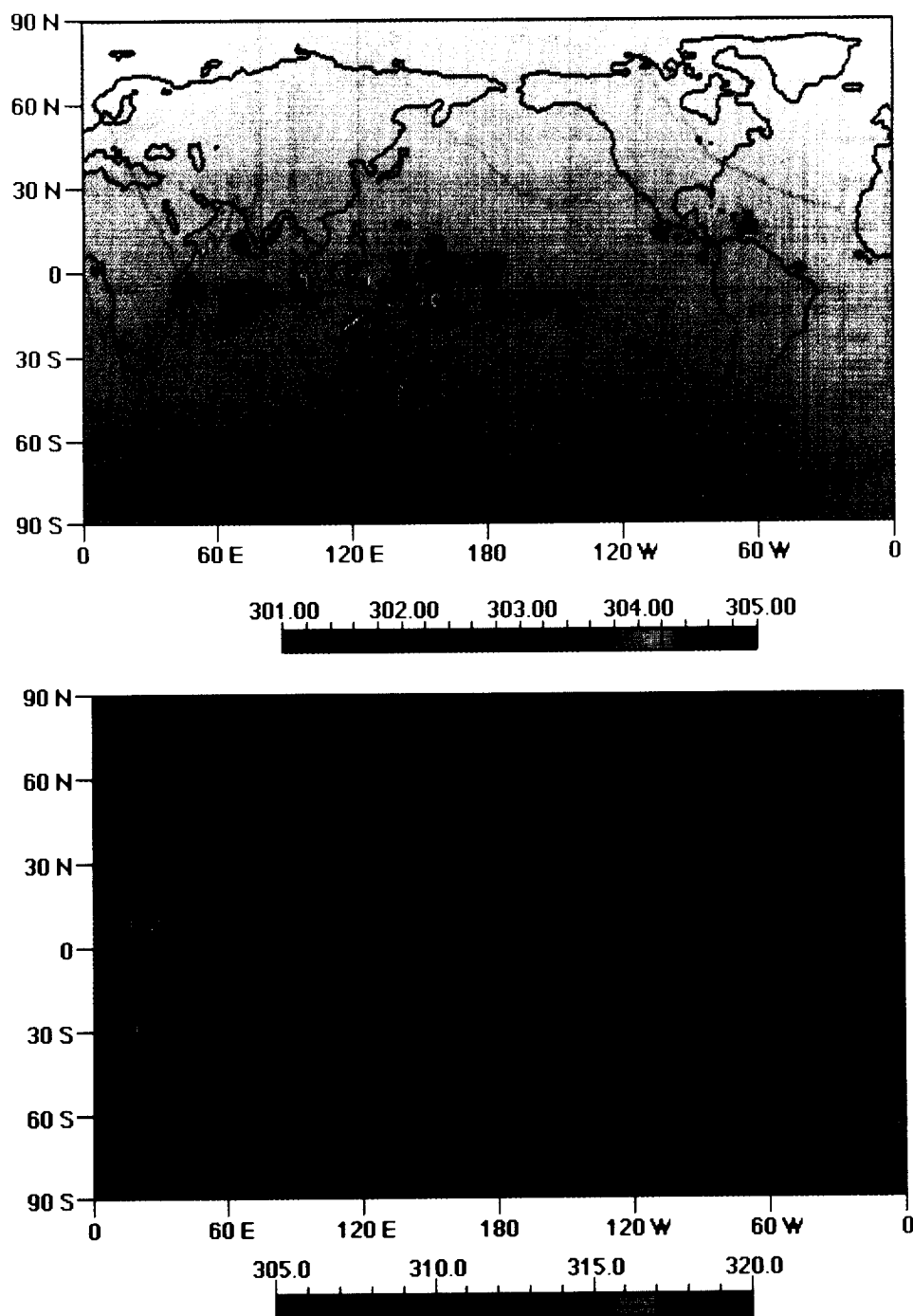


**Plate 1.** Location of the observed warm ocean pools in (top) the equatorial Pacific and (bottom) the hot desert spots in Africa and Australia as observed on January 4, 1979. Linear kriging [Isaaks and Srivastava, 1989] was applied to the observational data to underscore the patterns of spatial continuity and enhance the visual appearance of the clusters of warm and hot points.

*Tselioudis et al.* [1992]. In the range between 300 and 304 K the correlations are positive;  $\alpha$  increased by 40% and the cloud top heights reached their maximum levels. However, these positive correlations appear to reverse above 304 K with noticeable decrease in PWV in the upper troposphere. A similar event showing reversal of highly reflective clouds at high SSTs was also noted by *Waliser et al.* [1993] and

*Waliser and Graham* [1993]. Their critical SST value was placed at 302–303 K on an average monthly basis which compares well with the range of  $304 \pm 1$  K observed on a daily basis in this study.

The relationships between clouds and water vapor depend not only on the highest value of the SST but also on the size of the clusters of very high SSTs. For example, the Indian

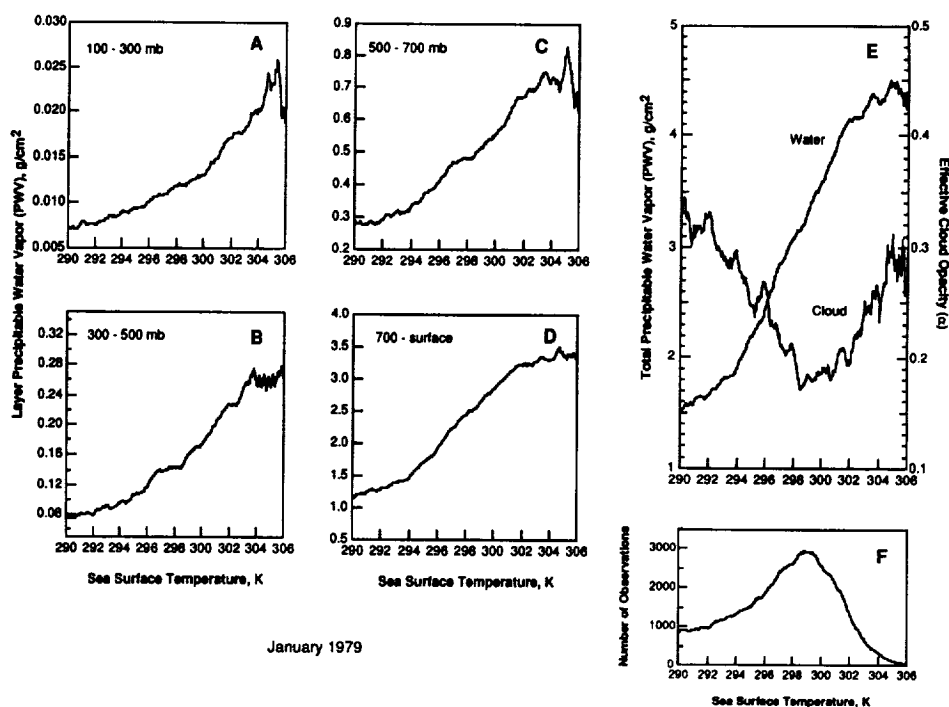


**Figure 1.** (a, b, c, and d) Daytime dependence of precipitable water vapor (PWV) in four atmospheric layers on variations of daily sea surface temperature (SST) across the warm pools (SST > 300 K) and their surroundings in the equatorial Pacific Ocean during the month of January 1979. The total PWV and the corresponding distribution of the effective infrared cloud opacity,  $\alpha$ , are shown in Figure 1e. A moving average of 0.5°C was applied to both PWV and  $\alpha$  to reduce uncertainties in the accuracy of SSTs. The number of cumulative observations corresponding to each value of SST in Figure 1f is given in steps of 0.05°C. There are 992 observations above 304 K.

Ocean in general exhibits very small warm clusters (Plate 1 (top)) and shows smaller increases in both PWV and  $\alpha$  as a function of increased SSTs.

There is much controversy regarding the feedbacks be-

tween upper tropospheric moisture and greenhouse warming and the processes which limit the rise in SST [Lindzen and Nigam, 1987; Raval and Ramanathan, 1989; Ramanathan and Collins, 1991; Rind et al., 1991; Fu et al., 1992; Wallace,

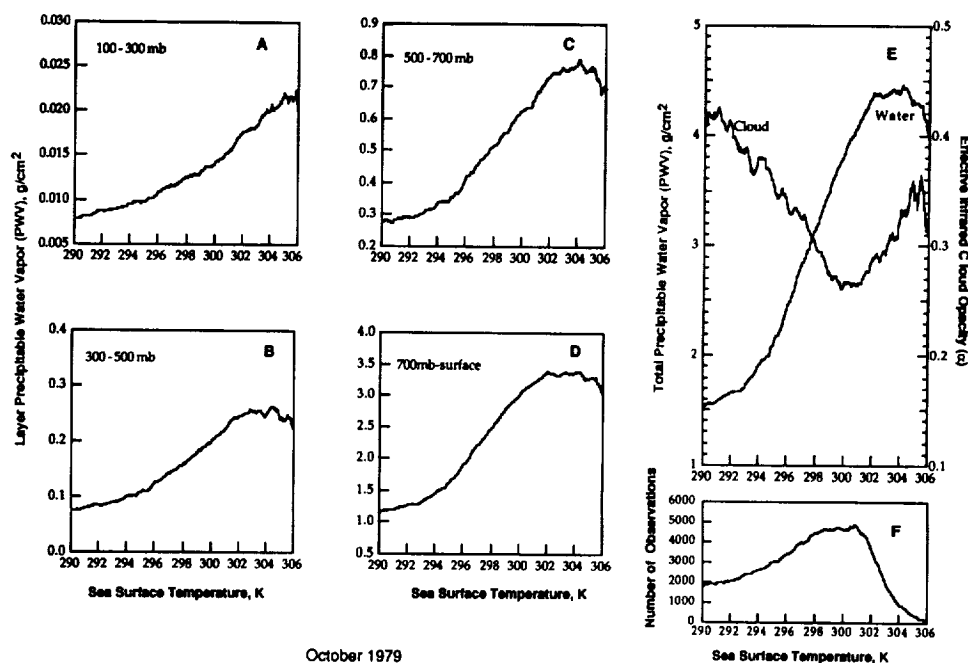


**Figure 2.** Same as for Figure 1 but for the month of October 1979. There are 1447 observations above 304 K.

**Table 1.** Observed Cloud Parameters for January 1979 Corresponding to a Representative Set of Ocean and Desert Surface Temperatures

Ocean			Land		
Surface Temperature	Cloud Top Pressure, mbar	Cloud Top Temperature, K	Surface Temperature	Cloud Top Pressure, mbar	Cloud Top Temperature, K
296.00	532.00	267.35	296.00	409.00	256.03
300.00	434.00	260.53	300.00	427.00	258.78
302.00	368.00	252.86	305.00	402.00	255.59
303.00	345.00	249.65	310.00	493.00	265.81
304.00	326.00	246.75	315.00	479.00	264.73
305.00	298.00	241.99	320.00	478.00	264.48

The tabulated data are binned uniformly at 1°C for both ocean and land. (Note that these values may differ from the 0.5°C binned values for oceans shown in Figures 1 and 2).

1992; Arking and Ziskin, 1994; Inamdar and Ramanathan, 1994]. Lindzen [1990] proposed that the flow field over the warm pool provides convergence of warm humid air in the boundary layer and the excess energy of condensation heating in the clouds is removed by the divergence of the flow of air at the higher levels. The resulting decrease in upper level moisture will increase radiation to space and thus reduce the magnitude of greenhouse warming. However, in spite of the flow divergence at the upper levels, moisture in the upper troposphere was observed to increase with increasing SST (up to  $304 \pm 1$  K). This increase was not confined to a single region and was widely observed in the western Pacific ( $150^\circ\text{E}$  to  $180^\circ$  and  $20^\circ\text{N}$  to  $20^\circ\text{S}$ ), eastern Pacific ( $180^\circ$  to  $150^\circ\text{W}$  and  $20^\circ\text{N}$  to  $20^\circ\text{S}$ ), and the Indian Ocean ( $60^\circ\text{E}$  to  $90^\circ\text{E}$  and  $0^\circ$  to  $20^\circ\text{S}$ ). In all three regions, for SSTs between 299 and 300 K, the total PWV was comparable, equal to  $3.9 \pm 0.2$  g/cm<sup>2</sup>, while the PWV in the 100- to 300-mbar layer was  $0.015 \pm 0.001$  g/cm<sup>2</sup>, well within the retrieval uncertainties. Consistent with these results, Rind *et al.* [1991] have also shown that upper atmospheric moisture is higher in the summer season of each hemisphere than in the winter season.

Graham and Barnett [1987] and Ramanathan and Collins [1991] proposed that the sharp increase in high-level clouds over the warm ocean pools acts both convectively and radiatively to produce a negative feedback which contributes to limiting the SSTs. Examination of the local relationships in Figure 1 between SST and  $\alpha$  together with the associated cloud top pressure and temperature given in Table 1 (as proxies for deep convection) indicates that the intensity of deep convection in the tropical Pacific increases with increasing sea surface temperature as SST rises above 300 K but with increases in SSTs above 304 K having less effect on the development of convection. This increase in convective activity derives from the fact that the variance in temperature lapse rate across the tropical troposphere is small, allowing the warmest saturated air parcels in the boundary layer to ascend into the highest levels in the troposphere. In addition, the results in Figures 1e and 2e indicate that extreme SST values occur only under conditions of diminished convection. This is indicated by the sharp net decrease in PWV above 700 mbar, especially above 300 mbar at SSTs above 304 K. But above 304 K the increase in PWV between 700 mbar and the surface observed in January and April could be due to continued evaporation (see Newell [1979] and Fu *et al.* [1992] on evaporation processes). Thus appar-

ently in the regime between 300 and 304 K, enhanced convection acts to control the rise in SST [Ramanathan and Collins, 1991], while in the second regime of diminished convection above 304 K the decrease in upper tropospheric moisture and the continuing surface evaporation are the most likely factors controlling the rise in SST.

#### 4. Hot Desert Spots

The data shown in Figures 3 and 4 describe the distribution of moisture and clouds as a function of LST of hot desert spots (Plate 1 (bottom)). Because the error in the derived land surface temperature is estimated to be at least  $\pm 1^\circ\text{C}$ , we applied a  $1^\circ\text{C}$  moving average to the individual data points in steps of  $0.05^\circ\text{C}$ . As in the case of the ocean data, this step reduced the scatter in the individual daily data points by about 20% for humidity and 50% for the cloud infrared opacity. The increase in surface temperature above 304 K is coupled with the rapid decrease in the total PWV (Figures 3e and 4e). Between 304 and 320 K the PWV decreased by 30% in the layer between the surface and 700 mbar and 20% between 300 and 100 mbar. The effective cloud opacity decreased to a minimum of 0.19 at 320 K.

The surface albedo, vegetation, soil dryness, and the general circulation of the atmosphere all interact to affect the local cloud cover, moisture, and rainfall over land. At this time, there is no scientific consensus on what triggers and maintains deserts and the observational data alone do not separate causes and effects. The feedback model proposed by Charney [1975] remains the leading explanation of the links between desert surface conditions and atmospheric moisture, clouds, and rainfall. According to the Charney model, the high surface albedo of dry, light, and arid deserts decreases the net radiation at the surface and increases the radiative cooling of the air above. As a result, air sinks in order to maintain thermal equilibrium, and cloudiness and precipitation are diminished. Low-level subsidence reduces moisture in the boundary layer and thus limits the moisture available in the atmospheric column, as observed in Figures 3 and 4. Furthermore, reduced moisture and precipitation adversely affect vegetation which in turn increases surface albedo further. This positive feedback was confirmed in subsequent modeling studies [Charney *et al.*, 1977; Walker and Rowntree, 1977; Shukla and Mintz, 1982; Cunningham and Rowntree, 1986] which showed that surface aridity and the accompanied subsidence and low atmospheric humidity contribute to the persistence of desert conditions.

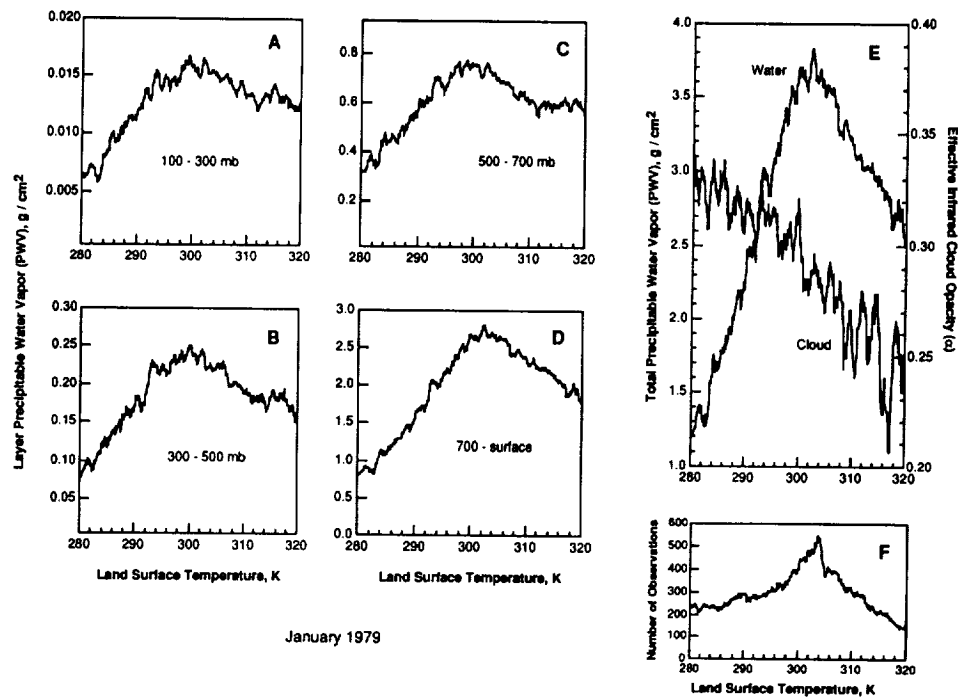


**Figure 3.** (a, b, c, and d) Daytime variations of PWV in four atmospheric layers as a function of daily values of land surface temperature (LST) across the hot spots ( $LST > 305$  K) and their surroundings during the month of January 1979. Desert total PWV and the corresponding distribution of the effective infrared cloud opacity,  $\alpha$ , are shown in Figure 3e. A moving average of  $1^\circ\text{C}$  was applied to both PWV and  $\alpha$  to reduce uncertainties in the accuracy of LSTs. The number of observations corresponding to each value of LST in Figure 3f is given in steps of  $0.05^\circ\text{C}$ . The data are truncated at 320 K because of large uncertainties in the accuracy of very high LST values and the small number of corresponding observations.

The results in Figures 3 and 4 were observed, with varying degrees, over hot tropical and subtropical deserts such as the Sahara, Kalahari, and central Australia, higher-latitude deserts in continental interiors such as the Gobi and Kaza-

khstan in central Asia, as well as deserts found on the western coasts of Africa and South America such as the Namib and the Atacama. However, unlike the general (semi-permanent) nature of the observations noted over the west-

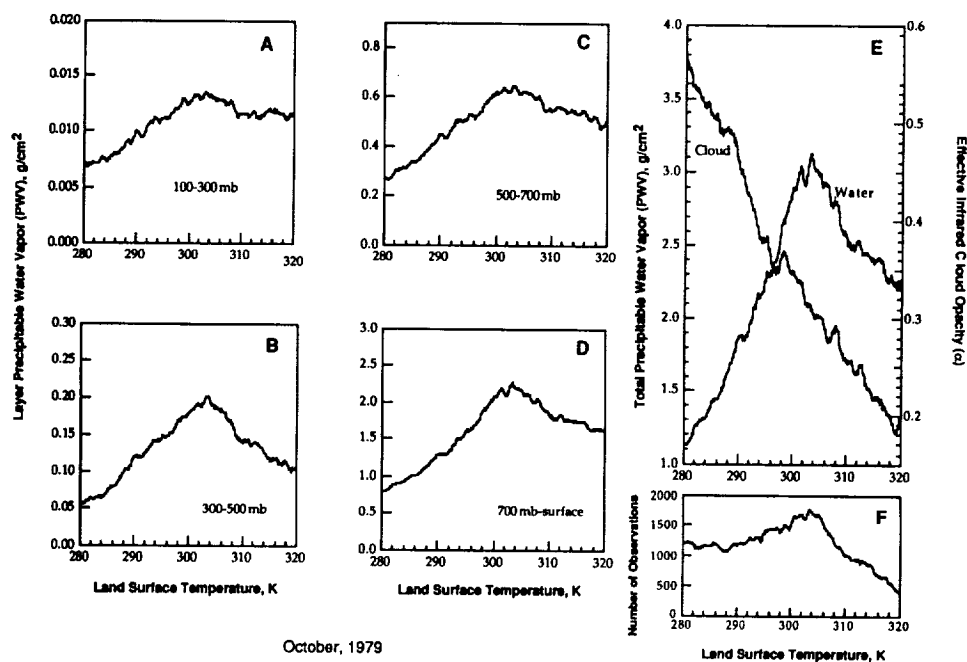


**Figure 4.** Same as for Figure 3 but for the month of October 1979.



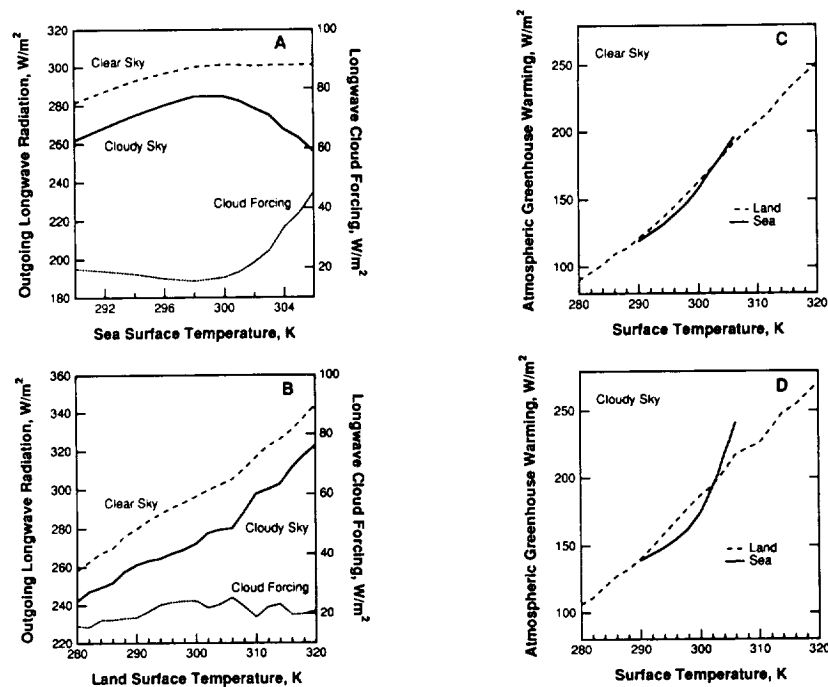


**Figure 5.** Calculated daytime outgoing longwave radiation (OLR) at the top of the atmosphere for the cases of the warm ocean pools and the hot desert spots discussed in Figures 1 and 3. The clear-sky OLR, the (observed) cloudy-sky OLR, and their difference (the cloud forcing) are shown in Figures 5a and 5b. The atmospheric greenhouse warming, defined as the difference between the surface emission  $\sigma T^4$  and the OLR, is shown in Figure 5c for clear-sky conditions and in Figure 5d for cloudy-sky conditions. (The data are binned uniformly at 1°C for both ocean and land.)

ern Pacific warm pools, the results obtained over the hot desert spots showed dependence on seasons, but no reversal in trends even when seasonal variations in insolation reduced the maximum LST of desert hot spots to less than 310 K. The dependence on seasons is to be expected because most desert regions are located near descending branches of Hadley cells, which vary with seasons and sometimes become weak and even vanish. Thus the stability of the observed trends must be maintained by the surface conditions.

## 5. Longwave Fluxes

A one-dimensional low-resolution radiation model [Kneizys *et al.*, 1988], LOWTRAN 7, was used to examine the relationship between longwave fluxes and surface temperature on the basis of the temperature, moisture, and cloud data derived for this study. The cloud infrared opacity was assumed constant across the spectrum. The specific humidity profile (in grams per kilogram) was determined under the assumption that the relative humidity is constant in each of the four observed layers and a fixed value of 0.002 g/kg was assumed above 100 mbar. The use of different linear approximations to derive the distribution of specific humidity within each layer had a very small effect on the calculated outgoing longwave radiation (OLR) (in the range of 0.1%) provided that the observed amount of precipitable water vapor in each layer is conserved. Note that the data used for the flux computations shown in Figure 5 were binned uniformly at 1°C for both ocean and land, similar to Table 1.

The contrast in the cloud-moisture relationships over

ocean and desert regions, illustrated in Figure 5, is very striking. Over the ocean the OLR for clear-sky conditions increased with increasing SST from 290 to 300 K, leveling off at 300 K in spite of the increased surface emission (Figure 5a). This is a result of the sharp rise in atmospheric moisture above 300 K, resulting in enhanced atmospheric absorption at the expense of OLR. By contrast, hot desert spots (Figure 5b) show a continuous increase in OLR which is directly traceable to the sharp increase in the desert surface temperature (the temperature lapse-rate effect) and the simultaneous decrease in water vapor absorption.

The atmospheric greenhouse warming is defined as the difference between surface emission ( $\sigma T^4$ ) and OLR. This difference increased with surface temperature for both ocean and land but for different reasons. Over deserts, while the fraction of the surface emission absorbed by the atmosphere decreased because of reduced moisture, the emission from the surface increased much faster (as  $\sigma T^4$ ), resulting in a net increase in the atmospheric greenhouse warming (Figure 5c). It is very interesting to note that for clear-sky conditions the atmospheric greenhouse warming is nearly identical over both land and ocean for the same surface temperatures between 290 and 304 K. The infrared cloud effect, shown in Figure 5d, amplified the atmospheric greenhouse warming even further, especially over the ocean.

## 6. Discussion

Although the use of observations to study and understand climate feedback processes is indispensable, it is generally impossible to separate causes and effects without the appli-

cation of models. At issue for both oceans and deserts is the need to isolate and quantify the relative contributions of atmospheric moisture, clouds, and surface conditions to the feedback processes. This is a prerequisite to explaining the observed common critical surface temperature of  $304 \pm 1$  K at which the PWV reaches a maximum value over both oceans and land.

At present, there is still significant contention as to whether convection-induced radiation or turbulent heat flux play the dominant role in limiting the rise in SSTs. The results of this study suggest that several interacting processes (like multiple safety valves) act simultaneously in the atmosphere and at the surface to limit the rise in SST. Deep convection appears to limit the daily (skin) SST of the tropical oceans to 304 K. In those very few spots where the convection effect breaks down, continued evaporation coupled with decreased upper tropospheric water vapor appear to be the most likely mechanisms limiting the rise of SST.

Similarly, over deserts the descending branches of the Hadley cells and the high surface albedo appear to reinforce each other to maintain existing desert conditions. An important question is whether maintenance of deserts is mostly a result of the Hadley circulation or the albedo feedback. Since the albedo feedback persists all year, while the intensity and location of the Hadley cell changes significantly, the results show the strong role of albedo in maintaining atmospheric subsidence and dryness (and so also surface aridity and lack of vegetation).

Finally, the results presented here describe mainly local convective events, but they bear noticeable resemblance to the large-scale tropical circulation of El Niño discussed by Ramanathan and Collins [1991]. How these two phenomena are linked together and how they may change as a result of increased  $\text{CO}_2$  is not obvious. Undoubtedly, increased global warming will increase convection, but unlike the large-scale tropical circulation, the extent of increased, small-scale convection depends strongly on the rate of increase of the local gradient of SSTs. Understanding these links requires further theoretical and observational studies.

## Appendix: Accuracy and Characteristics of Observational Data

The HIRS/MSU instruments are multichannel sounders which measure the Earth's outgoing radiance at frequencies selected to characterize different levels of the atmosphere. The HIRS instrument has 19 infrared channels between 3 and  $15 \mu\text{m}$  and one (uncalibrated) channel in the visible. The observed radiances in these infrared channels are affected by a number of atmospheric and surface parameters such as temperature, moisture, clouds, and ocean and land surfaces. The MSU has four channels in the 50-GHz region which are influenced mostly by atmospheric temperature and the surface. Unlike the infrared channels, the microwave channels are not influenced by most types of clouds.

The algorithm employed here is based on the relaxation method of solution of the full radiative transfer equation [Chahine, 1972]. By combining the analysis of the microwave and infrared channels, the algorithm produces accurate temperature and moisture profiles even in the presence of clouds, without requiring any field of view to be clear [Susskind et al., 1984]. The solutions were derived for spatial

grids of  $1^\circ$  latitude by  $1.25^\circ$  longitude, then averaged over larger grids of  $2^\circ$  latitude by  $2.5^\circ$  longitude, to reduce noise.

The accuracy of the derived temperature profiles with respect to radiosondes varied from  $1.8^\circ\text{C}$  for the least cloudy cases to  $2.0^\circ\text{C}$  for the cloudiest conditions. The mean monthly distribution of the total PWV shows agreement near 20% with colocated radiosondes [Barnett et al., 1991]. The largest discrepancies in PWV occur over land. The accuracy of the mean monthly SST is estimated [Susskind et al., 1985] to be  $\pm 0.5^\circ\text{C}$ . The space-derived SSTs refer to the radiation temperature of the surface, which could differ significantly from the customary ship measurements.

Validation studies of LSTs and cloud top heights are more difficult to achieve directly because of lack of field measurements. The error in LST is estimated to vary from  $\pm 1^\circ\text{C}$  for surface temperatures below 310 K to  $\pm 3^\circ\text{C}$  for temperatures of 320 K. Above 325 K the accuracy of LST is unknown. As to the effective cloud opacity, an indirect validation [Wu and Susskind, 1990] obtained by comparing the computed global OLR for the retrieved HIRS/MSU results with that from the Earth Radiation Budget data for 1979 showed a spatial standard deviation of approximately  $6 \text{ W/m}^2$ . This agreement is good evidence that the retrieved cloud and surface parameters are sufficiently accurate because of the large dependence of OLR on surface and cloud parameters. For example, for conditions with high clouds and 0.50 cloud opacity an error of  $6 \text{ W/m}^2$  can result from an error of 0.5 km in cloud top height and only 0.02 in cloud opacity, assuming that these are the only sources of error.

**Acknowledgments.** I thank R. Haskins for processing and validation of the data, D. Vane for discussions and support in preparing this paper, and D. Rind and P. Rowntree for their comments and suggestions. The HIRS/MSU data used in this paper were obtained from the NASA Goddard Space Flight Center. The research described in this paper was supported by the Jet Propulsion Laboratory, California Institute of Technology, under a contract with the National Aeronautics and Space Administration.

## References

- Arking, A., and D. Ziskin, Relationship between clouds and sea surface temperatures in the western tropical Pacific, *J. Clim.*, 7, 988–1000, 1994.
- Barnett, T. P., R. Haskins, and M. Chahine, Determination of the greenhouse gas signal from space: A progress report, *Adv. Space Res.*, 11(3), (3)37–(3)44, 1991.
- Chahine, M. T., A general relaxation method for inverse solution of the full radiative transfer equation, *J. Atmos. Sci.*, 29(4), 741–747, 1972.
- Chahine, M. T., Remote sounding of cloudy atmospheres, 1, The single cloud layer, *J. Atmos. Sci.*, 31(1), 233–243, 1974.
- Chahine, M. T., Remote sensing of cloud parameters, *J. Atmos. Sci.*, 39, 159–170, 1982.
- Chahine, M. T., The hydrological cycle and its influence on climate, *Nature*, 359, 373–380, 1992.
- Charney, J. G., Dynamics of deserts and drought in the Sahel, *Q. J. R. Meteorol. Soc.*, 101, 193–202, 1975.
- Charney, J., W. J. Quirk, S.-H. Chow, and J. Kornfield, A comparative study of the effects of albedo change on drought in semi-arid regions, *J. Atmos. Sci.*, 34, 1366–1385, 1977.
- Cunnington, W. M., and P. R. Rowntree, Simulations of the Saharan atmosphere—Dependence on moisture and albedo, *Q. J. R. Meteorol. Soc.*, 112, 971–999, 1986.
- Fu, R., A. D. Del Genio, W. B. Rossow, and W. T. Liu, Cirrus-cloud thermostat for tropical sea surface temperatures tested using satellite data, *Nature*, 358, 394–397, 1992.
- Graham, N. E., and T. P. Barnett, Sea surface temperature, surface

- wind divergence, and convection over the tropical oceans, *Science*, 238, 657–659, 1987.
- Hartmann, D. L., and D. A. Doelling, On the net radiative effectiveness of clouds, *J. Geophys. Res.*, 96, 869–891, 1991.
- Inamdar, A. K., and V. Ramanathan, Physics of greenhouse effect and convection in warm oceans, *J. Clim.*, 7, 715–731, 1994.
- Isaaks, E. H., and R. M. Srivastava, *Applied Geostatistics*, pp. 278–291, Oxford University Press, New York, 1989.
- Kiehl, J. T., and B. Briegleb, Comparison of the observed and calculated clear sky greenhouse effect: Implications for climate studies, *J. Geophys. Res.*, 97, 10,037–10,049, 1992.
- Kneizys, F. X., E. P. Shuettl, L. W. Abreu, J. H. Chetwynd, G. P. Anderson, W. O. Gallery, J. E. A. Shelby, and S. A. Clough, User's guide to LOWTRAN7, interim scientific report, *AFGL-TR 88-0177*, Air Force Geophys. Lab., 1988.
- Lindzen, R. S., Some coolness regarding global warming, *Bull. Am. Meteorol. Soc.*, 71(3), 288–299, 1990.
- Lindzen, R. S., and S. J. Nigam, On the role of sea-surface temperature-gradients in forcing low level winds and convergence in the tropics, *J. Atmos. Sci.*, 44, 2418–2436, 1987.
- Newell, R. E., Climate and the ocean, *Am. Sci.*, 67, 405–416, 1979.
- Phillips, N., J. Susskind, and L. McMillin, Results of a joint NOAA/NASA sounder simulation study, *J. Atmos. Oceanic Technol.*, 5, 44–56, 1988.
- Ramanathan, V., and W. Collins, Thermodynamic regulation of ocean warming by cirrus clouds deduced from observations of the 1987 El Niño, *Nature*, 351, 27–32, 1991.
- Raval, A., and V. Ramanathan, Observational determination of the greenhouse effect, *Nature*, 342, 758–761, 1989.
- Rind, D., W.-W. Chiou, W. Chu, J. Larsen, S. Oltmans, J. Lerner, M. P. McCormick, and L. McMaster, Positive water vapour feedback in climate models confirmed by satellite data, *Nature*, 349, 500–503, 1991.
- Schluessel, P., H.-Y. Shin, W. J. Emery, and H. Grassl, Comparison of satellite-derived sea surface temperatures with in situ skin measurements, *J. Geophys. Res.*, 92, 2859–2874, 1987.
- Shukla, J., and Y. Mintz, Influence of land-surface evapotranspiration on the Earth's climate, *Science*, 215, 1498–1500, 1982.
- Smith, W. L., and H. M. Woolf, The use of eigenvectors of statistical covariance matrices for interpreting satellite sounding radiometer measurements, *J. Atmos. Sci.*, 33, 70–83, 1976.
- Smith, W. L., H. M. Woolf, C. M. Hayden, D. Q. Wark, and L. M. McMillin, The Tiros-N operational vertical sounder, *Bull. Am. Meteorol. Soc.*, 60, 1172–1187, 1979.
- Susskind, J., and D. Reuter, Retrieval of sea surface temperatures from HIRS2/MSU, *J. Geophys. Res.*, 90, 1602–1608, 1985.
- Susskind, J., J. Rosenfield, D. Reuter, and M. T. Chahine, Remote sensing of weather and climate parameters from HIRS2/MSU on TIROS-N, *J. Geophys. Res.*, 89, 4677–4697, 1984.
- Tselioudis, G., W. B. Rossow, and D. Rind, Global patterns of cloud optical thickness variation with temperature, *J. Clim.*, 5, 1484–1495, 1992.
- Waliser, D. E., and N. E. Graham, Convective cloud systems and warm-pool sea surface temperatures: Coupled interactions and self-regulation, *J. Geophys. Res.*, 98, 12,881–12,893, 1993.
- Waliser, D. E., N. E. Graham, and C. Gautier, Comparison of highly reflective cloud and outgoing longwave radiation datasets for use in estimating tropical deep convection, *J. Clim.*, 6, 331–353, 1993.
- Walker, J., and P. R. Rowntree, The effect of soil moisture on circulation and rainfall in a tropical model, *Q. J. R. Meteorol. Soc.*, 103, 29–46, 1977.
- Wallace, J. M., Effect of deep convection on the regulation of tropical sea surface temperature, *Nature*, 357, 230–231, 1992.
- Wielicki, B., and R. N. Green, Cloud identification for ERBE radiative flux retrievals, *J. Appl. Meteorol.*, 28(11), 1133–1146, 1989.
- Wu, M.-L. C., and J. Susskind, Outgoing longwave radiation computed from HIRS2/MSU soundings, *J. Geophys. Res.*, 95, 7579–7602, 1990.

M. T. Chahine, Jet Propulsion Laboratory, California Institute of Technology, 4800 Oak Grove Drive, Mail Code 180-904, Pasadena, CA 91109-8099.

(Received March 10, 1994; revised October 25, 1994; accepted January 6, 1995.)

